

Compton Heated Outflow from CDAFs

Myeong-Gu Park

*Department of Astronomy and Atmospheric Sciences, Kyungpook National University,
Daegu 702-701, KOREA*

mfp@knu.ac.kr

and

Jeremiah P. Ostriker

*Princeton University Observatory, Princeton University, Princeton, NJ 08544;
Institute of Astronomy, Cambridge, UK*

jpo@astro.princeton.edu

ABSTRACT

Convection-dominated accretion flows (CDAF) are expected to have a shallower density profile and a higher radiation efficiency as compared to advection-dominated accretion flows (ADAF). Both solutions have been developed to account for the observed properties of the low luminosity, high temperature X-ray sources believed to involve accretion onto massive black holes. Self-similar CDAFs also have steeper poloidal density gradients and temperature close to the virial temperature. All these characteristics make CDAFs more capable of producing polar outflows driven by inverse Compton heating as compared to ADAF or to other classical accretion disks. We investigate the conditions for producing such outflows in non-magnetic CDAFs and look for the mass accretion rate, or, equally, the luminosity of CDAFs for which outflows exist. When the electron temperature saturates around 10^{11} K at the inner region, polar outflows are possible for $8 \times 10^{-7} \lesssim L/L_E \lesssim 4 \times 10^{-5}$, where L_E is the Eddington luminosity. Outflows are well collimated with small opening angles. The luminosity range for which outflow solutions exist is narrower for lower electron temperature flows and disappears completely for electron temperature $\lesssim 6 \times 10^9$ K. The tendency for jet like collimated outflows for these solutions is presumably astrophysically relevant given the high frequency of jets from AGNs.

Subject headings: accretion, accretion disks — black hole physics — quasars: general — X-rays: general

1. Introduction

Advection-dominated accretion flows (ADAF) nicely complement the classic thin disk accretion flows (Shakura & Sunyaev 1973; Ichimaru 1977; Rees et al. 1982; Narayan & Yi 1994, 1995; Abramowicz et al. 1995), and have been successfully applied to variety of cosmic objects, from galactic X-ray binaries to diffuse X-ray background (see Narayan, Mahadevan, & Quataert 1999 for review). However, analytic studies of ADAFs indicated the convectively unstable nature of ADAFs (Narayan & Yi 1994, 1995a; see Begelman & Meyer 1982 for radiation-dominated ADAF), which has subsequently been proved in a series of numerical simulations (Igumenshchev, Chen, & Abramowicz 1996; Igumenshchev & Abramowicz 1999, 2000; Stone, Pringle, & Begelman 1999; Igumenshchev, Abramowicz, & Narayan 2000). Especially, the numerical studies of ADAFs by Igumenshchev & Abramowicz (1999, 2000) show that an ADAF becomes a convection-dominated accretion flow (CDAF) whenever the viscosity parameter $\alpha \lesssim 0.1$. Further analyses of self-similar CDAF solutions show their unique properties (Narayan, Igumenshchev & Abramowicz 2000, hereafter NIA; Quataert & Gruzinov 2000, hereafter QG): the density varies as $\rho \propto R^{-1/2}$ (R is the radius), much flatter than the usual $R^{-3/2}$ in an ADAF or in spherical accretion. Correspondingly, the mean radial velocity varies as $v \propto R^{-3/2}$, compared to $R^{-1/2}$ in ADAF or in spherical flow. Energy generated at the inner part of the flow is transported to the outer part by convection. A CDAF has perhaps as much resemblance to the rotating stellar envelope of a massive star as to the usual accretion flow.

The other aspect of the two-dimensional nature of ADAF or CDAF solutions, often neglected, is the interaction between the outflowing radiation produced at smaller radii with the inflowing gas in the outer part of the flow. Of course in optically thick stars this interaction plays a vital role in establishing the equilibrium states. The radiative interaction also plays very important role in pure spherical accretion flows (Ostriker et al. 1976; Cowie, Ostriker, & Stark 1978; Wandel, Yahil, & Milgrom 1984; Park 1990a, 1990b; Nobili, Turolla, & Zampieri 1991; Zampieri, Miller, & Turolla 1996; Ciotti & Ostriker 1997, 2001). Park & Ostriker (1999, 2001) studied the same radiative interaction in the context of the ADAF solution and found that a polar outflow can be generated through Compton heating of electrons by high-energy photons emitted by the inner, hot part of the flow. The winds generated by the processes in the papers listed above are *not* momentum driven. Rather, they are caused by overheating of the gas in the slowly moving, low density polar regions. Outflows may also be generated from ADAF by other hydrodynamic processes (Narayan & Yi 1995; Xu & Chen 1997; Blandford & Begelman 1999).

In this work, we study the conditions for CDAFs to develop radiation driven outflows. We adopt the self-similar CDAF solution as the background flow structure (NIA; QG). The

treatment in this paper is two dimensional, adopting the angular profile of NIA and QG, except that the radiation field is simplified and treated as spherically symmetric.

2. Flow Properties

2.1. Density and Temperature

Multi-dimensional numerical simulations and analytic analyses show that density and temperature profiles of CDAF follow a self-similar form in radius (NIA; QG; Ball, Narayan & Quataert 2001, hereafter BNQ):

$$\rho(r) \propto r^{-1/2} \quad (1)$$

$$T_i(r) \propto r^{-1}, \quad (2)$$

where r is the radius in units of the Schwarzschild radius, $R_S \equiv 2GM/c^2 = 3.0 \times 10^5 m$ cm, and m is the black hole mass in solar units. This shallow radial dependence corresponds to marginal stability to convection; QG further show that the density should follow a power law in $\sin \vartheta$ (ϑ is the angle from the pole) while the temperature is constant on spherical shells. So we shall assume that the density is given by

$$\rho(r, \vartheta) = \rho_0 r^{-1/2} \sin^2 \vartheta \quad (3)$$

$$= \rho_{out} (r/r_{out})^{-1/2} \sin^2 \vartheta. \quad (4)$$

The flow extends from r_{out} down to $r_{in} = 1$, with the outer radius (analogous to the stellar photosphere) fixed by energy balance considerations.

The electron temperature, T_e , in an accretion flow is determined by the balance between various cooling and heating processes. In general, detailed studies of hot accretion flows (Narayan & Yi 1995b; Narayan, Barret, & McClintock 1997; BNQ) show that the electron temperature is equal to the ion temperature for $T_e \lesssim 10^9$ K, and then, at smaller radii, due to highly efficient relativistic bremsstrahlung and synchrotron emission, it flattens to somewhere between 10^9 K to 10^{11} K, depending on the amount of direct viscous heating to electrons. Hence, in this paper, we approximate the electron temperature as

$$T_e(r, \vartheta) = \frac{T_0}{r} \quad \text{for } r > r_1 \quad (5)$$

$$= T_1 \quad \text{for } r \leq r_1, \quad (6)$$

where $T_0 \approx 10^{12}$ K, T_1 is some constant between 10^9 K and 10^{11} K, and $r_1 \equiv T_0/T_1$.

From equation (3), we find that the Thomson optical depth to electron scattering within r is

$$\tau_{es}(r, \vartheta) = \frac{1}{2} \dot{m} r^{1/2} \sin^2 \theta, \quad (7)$$

where $\dot{m} \equiv \dot{M}/\dot{M}_E = \dot{M}c^2/L_E$ is the dimensionless mass accretion rate. Our analysis, which is to be applied to low accretion rate solutions, will assume that the flow is optically thin to both scattering and redistribution processes.

2.2. Radiation Field and Radiation Temperature

The inner part of the flow produces higher energy, Comptonized, relativistic bremsstrahlung photons, while the outer part produces lower energy bremsstrahlung photons. Hence the radiation field at a given position is determined by the contribution from inner radiating shells plus the outer shells. Although in each shell, the density, and therefore, the emissivity (i.e. cooling function) is a function of poloidal angle ϑ , the energy density is more uniform over angle than is the emissivity. So, for estimating the energy outflow, we will simplify the calculation of radiative transfer by assuming each radiating shell is homogeneous, using an angle average over the sphere.

Therefore, the radiation energy density at given r , $E_X(r)$, is given by

$$cE_X(r) = R_s \left[\frac{1}{4\pi r^2} \int_{r_{in}}^r \Lambda(r') 4\pi r'^2 dr' + \int_r^{r_{out}} \Lambda(r') \frac{r'}{r} \ln \sqrt{\frac{r' + r}{r' - r}} dr' \right], \quad (8)$$

where the first term is the contribution from inner radiating shells and the second term from outer radiating shells (see Appendix A). The emissivity per unit volume is denoted as the cooling function Λ , which will be described in §3.1.

For relativistic un-Comptonized bremsstrahlung, with $\Lambda \propto \rho^2 T_e$ and CDAF scaling $\rho \propto r^{-1/2}$ and $T_e \propto r^{-1}$, the incremental luminosity $dL_X(r)/dr = \text{constant}$, and the luminosity at a given radius r has the largest contribution from the outermost shell. Nevertheless, equation (8) gives a peak energy density in the inner region (cf. dashed line in Fig. 1) and a significant radiation pressure gradient. In addition, when there is strong Comptonization, the contribution from the inner region can be significantly enhanced.

Moreover, the amount of Compton heating is determined by the luminosity times the photon energy, and is largely dominated by the inner hot region. The radiation temperature, defined as $kT_X(r)$ being the energy-weighted mean photon energy, at a given radius r is

determined by the equation

$$cT_X(r)E_X(r) = R_S \left[\frac{1}{4\pi r^2} \int_{r_{in}}^r T_X(r')\Lambda(r')4\pi r'^2 dr' + \int_r^{r_{out}} T_X(r')\Lambda(r')\frac{r'}{r} \ln \sqrt{\frac{r'+r}{r'-r}} dr' \right]. \quad (9)$$

This quantity is more concentrated than $E_X(r)$, especially in the presence of strong Comptonization [see *dotted curve* in Fig. 1 for $T_X(r)$].

In presence of an overheated wind, some region along the pole in CDAF will not be able to accrete matter, while the remaining equatorial region normally accretes (see §3.3). In most of the relevant parameter space, the overheated ‘funnel’ is very narrow, and we assume (with regard to energy generation) that the self-similar CDAF flow is filling the whole space including the polar region, omitting the small correction due to the solid angle Ω_W (~ 0.2 sr) occupied by the outflowing wind/jet.

The resulting profiles of radiation moments and the radiation temperature show the aforementioned characteristics of CDAFs. The luminosity,

$$L(r) = R_S^3 \int_{r_{in}}^r \Lambda(r')4\pi r'^2 dr', \quad (10)$$

increases at large radius (*solid curve* in Fig. 1), while the radiation temperature is roughly flat or decreasing slowly outward after peaking at some intermediate radius (*dotted curve* in Fig. 1).

2.3. Outer Boundary

The simplest self-similar CDAF has zero mass accretion rate (NIA), and this of course corresponds to zero luminosity. However, the accretion flow must lose energy by radiative cooling, and this energy loss is very likely provided by the convective energy transport (NIA, BNQ). We follow BNQ to assume that the total luminosity of ADAF is proportional to the mass accretion rate:

$$L(r_{out}) = \eta_c \epsilon_c \dot{M} c^2, \quad (11)$$

where the convective efficiency ϵ_c , determined by numerical simulations to be in the range $\sim 10^{-2} - 10^{-3}$ and η_c is the fraction of convected energy to be radiated away by electrons. In subsequent examples, we nominally adopt $\epsilon_c \eta_c = 10^{-2}$ (BNQ). We also adopted smaller values of $\epsilon_c \eta_c$ or a scaling of $\epsilon_c \eta_c$ with \dot{m} (cf. §3.3), and the results were qualitatively the same.

We determine the outer boundary for a given mass accretion rate \dot{m} by finding the radius r_{out} at which equation (11) is satisfied. This gives a somewhat different relation between the total luminosity and the mass accretion rate from that in BNQ because we have used Comptonized relativistic bremsstrahlung while BNQ employ only un-Comptonized non-relativistic bremsstrahlung. However, the general characteristic of the relation is the same: higher mass accretion flows have smaller outer boundary radii. This is due to the special radial profile of density in CDAF solutions. Because of the weak density gradient with radius, most of the luminosity contribution is from the outer part of the flow, which makes CDAF flows quite distinct from other accretion flows including ADAFs. The dimensionless total luminosity, $L(r_{out})/L_E$, is directly proportional to the dimensionless mass accretion rate, $\dot{m} \equiv \dot{M}/\dot{M}_E$, by equation (11) while the luminosity accumulated from bremsstrahlung is very roughly proportional to $\dot{m}^2 r_{out}$ (with a higher power in \dot{m} if Comptonization is important). Since these two luminosities must be equal, a higher \dot{m} flow implies a smaller r_{out} (see *solid lines* in Fig. 2). Therefore lower mass accretion rate CDAF solutions have lower luminosity, yet are more extended, if we treat $\epsilon_c \eta_c$ as fixed, independent of \dot{m} .

3. Outflow

3.1. Cooling and Heating

The main cooling mechanism we consider in this work is Comptonized bremsstrahlung. This process is not only the source of electron cooling but also the source of the inverse Comptonizing radiation field.

The comptonized bremsstrahlung cooling rate per unit volume can be reasonably approximated by (Svensson 1982; Stepney & Guilbert 1983)

$$\Lambda_{br} = \sigma_T c \alpha_f m_e c^2 n^2 [F_{ei}(T_e) + F_{ee}(T_e)], \quad (12)$$

where

$$F_{ei} = 4 \left(\frac{2}{\pi^3} \right)^{1/2} \theta_e^{1/2} (1 + 1.781 \theta_e^{1.34}) \quad \text{for } \theta_e < 1 \quad (13)$$

$$= \frac{9}{2\pi} \theta_e [\ln(1.123 \theta_e + 0.48) + 1.5] \quad \text{for } \theta_e > 1$$

$$F_{ee} = \frac{5}{6\pi^{3/2}} (44 - 3\pi^2) \theta_e^{3/2} (1 + 1.1\theta_e + \theta_e^2 - 1.25\theta_e^{5/2}) \quad \text{for } \theta_e < 1 \quad (14)$$

$$= \frac{9}{\pi} \theta_e [\ln(1.123 \theta_e) + 1.2746] \quad \text{for } \theta_e > 1,$$

$\theta_e \equiv kT_e/m_e c^2$, n is the electron (ion) number density, σ_T the Thomson cross section, α_f the fine structure constant, and m_e the electron mass.

The emitted bremsstrahlung photons are upscattered by inverse Compton scattering. The amplification of photon energy by a single scattering is $A \equiv 1 + 4\theta_e + 16\theta_e^2$. The probability of single scattering is $P = 1 - \exp(-\tau_{es})$ (see e.g., Dermer et al. 1991). Therefore the mean amplification factor by Compton scattering would be

$$\eta_0 = 1 - P + PA = 1 + P(A - 1). \quad (15)$$

The fraction $1 - P$ of photons is not changed while the fraction P of photons are upscattered to A times their initial energy. This prescription is valid only for single scattering Comptonization. Since most CDAF flow considered here has $\tau_{es} < 1$, we use this amplification factor for Comptonized bremsstrahlung. Although Dermer et al. (1991) provides a handy formula for η , applicable to diverse regimes, it can give incorrect values for $A \gg 1$ and $\tau_{es} \lesssim 1$, the main parameter regime of CDAF. Although τ_{es} is a hard-to-define quantity in a complex flow, we simply adopt $\tau_{es} = n_e \sigma_T r$ in this work for the purpose of estimating the Comptonization.

When $PA \gg 1$, Comptonization becomes saturated, and all photons that are not absorbed are upscattered to $3T_e$, that is $\eta \rightarrow \eta_{sat} = 3\theta_e/x$ where $x \equiv h\nu/m_e c^2$ (Dermer et al. 1991). The fully saturated Comptonized bremsstrahlung is then

$$\Lambda_{Cbr}^{sat} = \int_{x_{abs}}^{3\theta_e} \eta_{sat} \epsilon_{br}(x) dx + \int_{3\theta_e}^{\infty} \epsilon_{br}(x) dx \quad (16)$$

$$= \Lambda_{br} \left[\int_3^{\infty} e^{-t} dt + \int_{x_{abs}/\theta_e}^3 3t^{-1} e^{-t} dt \right] \quad (17)$$

where $\epsilon_{br}(x)$ is the bremsstrahlung spectrum

$$\epsilon_{br}(x) = \Lambda_{br} \exp\left(-\frac{x}{\theta_e}\right) dx \quad (18)$$

and x_{abs} is the absorption frequency ν_{abs} in unit of $m_e c^2/h$. Since Λ_{br} is smaller by the factor $\exp(x_{abs}/\theta_e)$ in presence of absorption, we take the maximum amplification factor for bremsstrahlung as

$$\eta_{br}^{sat} = e^{x_{abs}/\theta_e} \times \left\{ e^{-3} + 3 \left[E_1\left(\frac{x_{abs}}{\theta_e}\right) - E_1(3) \right] \right\}, \quad (19)$$

where $E_n \equiv \int_1^{\infty} t^{-n} \exp(-xt) dt$ is the exponential integral. The final Comptonized bremsstrahlung emission is then

$$\Lambda_{Cbr} = \min(\eta_0, \eta_{br}^{sat}) \Lambda_{br}. \quad (20)$$

The energy-weighted mean photon energy for unsaturated Comptonized bremsstrahlung is (see e.g. PO2)

$$\frac{4kT_X}{m_e c^2} = \frac{\int_0^\infty \eta_{br}^2 x \epsilon_{br}(x) dx}{\int_0^\infty \eta_{br} \epsilon_{br}(x) dx} = \eta_{br} \theta_e, \quad (21)$$

and that for saturated Comptonized bremsstrahlung is simply

$$T_X = T_e, \quad (22)$$

since the spectrum approaches Wien spectrum which has $T_X = T_e$. Therefore, the radiation temperature of locally radiated bremsstrahlung emission is

$$T_X^{Cbr} = \frac{1}{4} T_e \min(\eta_{br}, 4). \quad (23)$$

The frequency ν_{abs} is chosen to be the frequency at which the free-free absorption optical depth is equal to 1,

$$ra_{ff}(\nu_{abs}) = 1, \quad (24)$$

where a_{ff} is the absorption coefficient given by Dermer et al. (1991)

$$a_{ff}(x) = \sqrt{8\pi} \frac{\alpha_f^2 \sigma_T r_e^3}{x^2 \theta_e^{3/2} \left[1 + (8/\pi)^{1/2} \theta_e^{3/2} \right]} n_i^2 \bar{g} \quad (25)$$

with

$$\begin{aligned} \bar{g} = & (1 + 2\theta_e + 2\theta_e^2) \ln \left[\frac{4\eta_E(1 + 3.42\theta_e)\theta_e}{x} \right] \\ & + \left(\frac{3\sqrt{2}}{5} + 2\theta_e \right) \theta_e \ln \left[\frac{4\eta_E(11.2 + 10.4\theta_e^2)\theta_e}{x} \right], \end{aligned} \quad (26)$$

α_f is the fine structure constant, and $r_e = e^2/m_e c^2$ the electron radius (Svensson 1984). This expression is valid for $x \ll \theta_e$ and we used $(\pi/2)^{1/2} \theta_e^{1/2} [1 + (8/\pi)^{1/2} \theta_e^{3/2}]$ to approximate $\exp(1/\theta_e) K_2(1/\theta_e)$.

Flow at a given position is heated (or cooled) by the inverse Comptonization off electrons. We use the heating rate (Levich & Sunyaev 1971)

$$\Gamma_C = 4\sigma_T c [\theta_X(r) - \theta_e(r)] E_X(r) n_e(r, \vartheta), \quad (27)$$

where $E_X(r)$ is the radiation energy density from equation (8) and $\theta_X \equiv kT_X/m_e c^2$ the radiation temperature from equation (9).

3.2. Equilibrium Temperature and Overheating

The thermal equilibrium is determined by the balance between inverse Compton heating and Comptonized bremsstrahlung cooling. Hence, the thermal equilibrium temperature T_{eq} satisfies

$$\Gamma_C(T_{eq}) = \Lambda_{Cbr}(T_{eq}) \quad (28)$$

at given position (r, ϑ) . From equations (20) and (27), $\theta_{eq} \equiv kT_{eq}/m_e c^2$ is determined from

$$4cE_X(r)[\theta_X(r) - \theta_{eq}] = \alpha_f m_e c^3 n_e(r, \vartheta) \eta_{Cbr}(n_e, r, \theta_{eq}) [F_{ei}(\theta_{eq}) + F_{ee}(\theta_{eq})]. \quad (29)$$

Since the number density $n_e(r, \vartheta)$ decrease as $\vartheta \rightarrow 0$ (toward the pole), the derived electron temperature increases toward the pole as long as $\theta_X > \theta_e$.

For smaller enough ϑ , the thermal equilibrium temperature can be higher than the virial temperature,

$$T_{eq}(r, \vartheta) > T_{vir}(r). \quad (30)$$

The virial temperature is defined as $(5/2)kT_{vir} = m_p GM/r$, where m_p is the proton mass. Once electrons are heated above the virial temperature, and therefore above the ion temperature, electrons are likely (via collisions and instabilities) to heat ions to above the virial temperature, thereby, creating winds, especially because the dynamical time of CDAF is much longer than the free-fall flow. Therefore, we adopt equation (30) as the condition for overheating and producing a wind.

There also is a trivial, yet additional constraint for overheating: the radiation temperature must be higher than the virial temperature

$$T_X(r) > T_{vir}(r). \quad (31)$$

3.3. Outflow

Outflows will extend from the polar axis to the angle ϑ_c at which the equilibrium temperature is equal to the virial temperature,

$$T_{eq}(r, \vartheta_c) = T_{vir}(r). \quad (32)$$

Regions with $\vartheta < \vartheta_c$ are overheated to above the virial temperature. Hence, the shape of the outflow is determined by the angle $\vartheta_c(r)$ as a function of r .

One example of the outflow is shown in Figure 3 for the mass accretion rate of $\dot{m} = 10^{-3}$, the electron temperature of inner region $T_1 = 10^{11}$ K. The *solid* curve shows $\vartheta_c(r)$, and the

outer dotted circle is the outer boundary of the flow. The outflow starts at $r \simeq 40$ and the opening angle ϑ_c reaches maximum of 17° around $r \simeq 700$ and ends with 8.3° at the outer boundary. Figure 4 shows the same for $\dot{m} = 2.0 \times 10^{-3}$ and $T_1 = 3.0 \times 10^{10}$ K with $\vartheta_c = 6.6^\circ$ at the boundary. The inner isothermal region and the immediate surroundings have $T_X < T_{vir}$, and the overheating does not occur. However, at larger radius Compton heating is strong enough to overheat the polar region of the gas and produce outflow. The fraction of the sphere covered by the outflowing gas is $2\pi\vartheta^2/4\pi \sim 0.01$ for $\vartheta = 8.3^\circ$.

We have considered combinations of \dot{m} and T_1 . Outflow solutions exist within a limited range of these parameters. Too high \dot{m} makes the outer boundary so small that the whole region is isothermal, and, therefore, $T_X = T_e$. The outer boundary is smaller for higher \dot{m} because radiative luminosity is proportional to \dot{m}^2 while CDAF flows have a fixed (assumed) radiation efficiency, which makes the total luminosity roughly proportional to \dot{m} . The only way to reconcile this is r_{out} being smaller for higher \dot{m} (BNQ). In a too low \dot{m} flow, Comptonization is not strong enough to keep the radiation temperature high. Lower energy photons from larger radii dilute the radiation field and flows are not heated. In Figure 5, we show region of space in (\dot{m}, T_1) where outflow solutions are successfully produced. Circles denote (\dot{m}, T_1) for which outflows are found. The size of circle represents the opening angle of the outflow at the outer boundary, the majority being $\lesssim 10^\circ$. Crosses denote (\dot{m}, T_1) values for which outflows do not exist.

As expected, flows with high electron temperature are more likely to develop outflows. Outflows are not expected for $T_1 < m_e c^2/k \simeq 6 \times 10^9$ K: Comptonization is less efficient when $kT_e/m_e c^2 < 1$. Since the adopted radiation efficiency is $\epsilon_c \eta_c \simeq 10^{-2}$, we expect CDAFs with outflows to exist in the luminosity range $8 \times 10^{-7} \lesssim L/L_E \lesssim 4 \times 10^{-5}$ for $T_1 = 10^{11}$ K and $4 \times 10^{-5} \lesssim L/L_E \lesssim 10^{-4}$ for $T_1 = 10^{10}$ K. These results do not depend on the mass of the black holes.

So far, we have assumed that the total radiation efficiency $\epsilon_c \eta_c$ is constant. In fact, current theoretical understanding of the CDAF solution is not yet secure on this point. We now relax that assumption and study an alternative case when $\epsilon_c \eta_c$ is assumed to be proportional to \dot{m} . We adopt simply $\epsilon_c \eta_c = 10^{-2}(\dot{m}/10^{-2})$ so as to make $\epsilon_c \eta_c = 10^{-2}$ for $\dot{m} = 10^{-2}$. Now for small \dot{m} the total luminosity determined from equation (11) and the total bremsstrahlung emission from equation (10) are both proportional to \dot{m}^2 , and the outer boundary is now at a roughly constant radius (see dotted lines in Fig. 2). At high \dot{m} , Comptonization adds additional power of \dot{m} to the total emission, and r_{out} depends on \dot{m} (see dotted lines in Fig. 2). The outflow solutions for this choice of radiation efficiency are shown in Figure 6. Qualitatively, they are not much different from the solutions with constant $\epsilon_c \eta_c$. Nonetheless, the flow is much less extended due to lower radiation efficiency

for lower \dot{m} and the shape of the outflow funnel in this case is almost straight. The whole flow structure is quite self-similar except for the magnitude of the opening angle. Most of the solutions still have the opening angle at the outer boundary $\lesssim 20^\circ$.

3.4. Synchrotron Emission

We have also studied CDAFs with significant magnetic field. We used the black hole mass of $10^8 M_\odot$ for the calculation. The treatment of Comptonized synchrotron is explained in Appendix B. We, however, have found that even a tiny amount of magnetic field, e.g. 1% of equipartition magnetic field, is enough to create sufficient number of soft synchrotron photons to lower the radiation temperature below the electron temperature. In other words, radiation cools the electrons rather than heats them in the presence of magnetic field. So we conclude that Compton preheated outflow does not exist in general magnetic CDAFs.

4. Summary and Discussion

Hot accretion flows like ADAFs have a number of physical characteristics that compliment the classic low-temperature disk flows. In previous work, we have explored the consequences of the high temperature and the two-dimensional density structure of these flows, and have found that ADAFs may be able to produce radiatively driven outflows. We subsequently have noted that self-similar CDAFs have even more suitable properties for producing outflows as compared to ADAFs: steeper poloidal density gradients and higher radiation efficiencies. In this paper, we have studied the conditions for self-similar two-dimensional CDAFs (NIA; QG) to develop radiatively heated polar outflows.

1. We have found that CDAFs produce enough luminosity and photon energy to drive polar outflows via inverse Compton heating for a reasonable range of mass accretion rate, or, equally, luminosity. When the electron temperature saturates around 10^{11} K at the inner region, polar outflows are possible for $8 \times 10^{-7} \lesssim L/L_E \lesssim 4 \times 10^{-5}$ for radiation efficiency of 10^{-2} , where L_E is the Eddington luminosity. The luminosity range for which outflow exists is narrower for lower electron temperature flows and disappears completely for electron temperature $\lesssim 6 \times 10^9$ K

2. In most cases, outflows are well collimated, with an opening angle typically in the range $\lesssim 10^\circ$.

3. If we, instead of taking efficiency as constant, assume that it is proportional to \dot{m} , the solutions are qualitatively the same but are more self similar, i.e., opening angle and

outer boundary (in Schwarzschild units) depend less strongly on \dot{m} .

4. In the presence of magnetic field, copious soft synchrotron photons would cool the flow rather than heat it, and preheated outflow would not occur, and the observed radiation temperatures are correspondingly reduced.

The treatment in this work is not completely satisfactory in the sense that the dynamics and the temperature profiles of CDAFs are not self-consistently solved. However, it was not our intention to solve fully three-dimensional, self-consistent global CDAFs with proper consideration for all gas, radiative, and magnetic processes, which will be eventually needed to fully understand CDAFs. Rather, our goal has been to show that even in the framework of simple self-similar solutions, radiatively heated polar outflows appear as natural consequences of the physical characteristics of CDAFs.

This work was supported by Korea Research Foundation Grant (KRF-2001-015-DP0610).

A. Radiation Field Inside An Optically Thin Spherical Shell

Let's consider an optically thin, uniform radiating shell with radius r' and the thickness $\Delta r'$. The specific intensity at radius r ($r < r'$) in the direction of ϑ (see Figure 7) is given by integration of radiative transfer equation along that direction. If we denote the emissivity (per unit volume per unit solid angle) of the shell as $\epsilon_\nu/4\pi$, then the specific intensity is simply the emissivity times the path length,

$$I_\nu = \frac{\epsilon_\nu}{4\pi} \Delta s = \frac{\epsilon_\nu}{4\pi} \frac{\Delta r'}{\cos \phi}, \quad (\text{A1})$$

where ϕ is the angle between the ray and the normal of the shell. From the law of sines, $\sin \phi = (r/R) \sin \vartheta$. The radiation energy density, $E_\nu(r)$, is given by the integral of I_ν over the solid angle $d\Omega$,

$$E_\nu(r) = \frac{1}{c} \int \frac{\epsilon_\nu}{4\pi} \frac{\Delta r'}{\cos \phi} d\Omega \quad (\text{A2})$$

$$= \frac{1}{c} \frac{\epsilon_\nu}{4\pi} \Delta r' \int \frac{\sin \vartheta d\vartheta}{\sqrt{1 - \frac{r^2}{r'^2} \sin^2 \vartheta}} d\varphi \quad (\text{A3})$$

$$= \frac{1}{c} \epsilon_\nu \Delta r' \frac{r'}{r} \ln \sqrt{\frac{r' + r}{r' - r}}. \quad (\text{A4})$$

Equation (A2) formally diverges when $r \rightarrow r'$ whereas the correct value saturates. In the limit when $r' - r \lesssim \Delta r'$, the effect of shell's curvature has to be incorporated in Δs . However,

since the radiation energy density is calculated by the sum of contributions from discrete shells in r (eq. [8]), the divergence is automatically avoided.

B. Comptonized Synchrotron Emission

The angle-averaged synchrotron emission by relativistic Maxwellian electrons is given by (Pacholczyk 1970)

$$\epsilon_{syn}(\nu)d\nu = \frac{2\pi}{\sqrt{3}} \frac{e^2}{c} \frac{n_e \nu}{\theta_e^2} I'(x_M) d\nu \quad (B1)$$

where $x_M \equiv 2\nu/(3\nu_0\theta_e^2)$, $\nu_0 \equiv eB/(2\pi m_e c)$, and

$$I'(x_M) = \frac{4.0505}{x_M^{1/6}} \left(1 + \frac{0.40}{x_M^{1/4}} + \frac{0.5316}{x_M^{1/2}} \right) \exp(-1.8899x_M^{1/3}) \quad (B2)$$

is a fitting formula (Mahadevan, Narayan, & Yi 1996). When absorption is not important, the cooling rate due to the optically thin synchrotron emission is obtained by integrating the equation (B1)

$$\Lambda_{syn}^0 = 213.6 \frac{e^2}{c} n_e \nu_0^2 \theta_e^2. \quad (B3)$$

However, a large fraction of the low energy synchrotron photons are generally absorbed by synchrotron self-absorption. The synchrotron emission in the presence of absorption can be approximated as

$$\Lambda_{syn} = f_{syn} \Lambda_{syn}^0, \quad (B4)$$

where

$$f_{syn} \equiv \int_{x_{abs}}^{\infty} x I'(x) dx / \int_0^{\infty} x I'(x) dx \quad (B5)$$

is the fraction of synchrotron emission above the absorption frequency ν_{abs} , and $x_{abs} = h\nu_{abs}/m_e c^2$. Thus, we only consider the optically thin part of synchrotron emission as the cooling function for the gas and as a contribution to the preheating radiation field.

Locally emitted synchrotron photons are upscattered by inverse Comptonization off hot electrons. Here, we adopt a simple estimate of Comptonized synchrotron, which is reasonable in physical conditions considered in this paper,

$$\Lambda_{CS} = \eta_{syn} f_{syn} \Lambda_{syn}^0, \quad (B6)$$

where

$$\eta_{syn} = \min(\eta_0, \eta_{syn}^{sat}) \quad (B7)$$

is the Comptonized energy enhancement factor (see e.g., Dermer et al. 1991) for synchrotron emission. The enhancement factor for fully saturated Comptonized synchrotron in the presence of absorption is

$$\eta_{syn}^{max} = \frac{\int_{x_{abs}}^{3\theta_e} \frac{3\theta_e}{x} x I'(x) dx}{\int_{x_{abs}}^{3\theta_e} x I'(x) dx}, \quad (B8)$$

(see §3.1 for bremsstrahlung case). The absorption frequency for synchrotron self-absorption from

$$\tau_{syn} = \frac{1}{4\sqrt{3}} \frac{e^2 c n_e(r) r}{\nu k T_e \theta_e^2} I'(x_M) = 1 \quad (B9)$$

is compared with that for free-free absorption, and the larger of the two is chosen.

The radiation temperature of locally emitted Comptonized synchrotron is similarly

$$T_X^{CS} = \min(\eta_0 \frac{3 h \nu_0}{8 k} \theta_e^2 \langle x_M \rangle_{\epsilon_\nu}, T_e), \quad (B10)$$

where

$$\langle x_M \rangle_{\epsilon_\nu} \equiv \frac{\int_{x_M^{abs}}^{\infty} x_M^2 I'(x_M) dx_M}{\int_{x_M^{abs}}^{\infty} x_M I'(x_M) dx_M} \quad (B11)$$

is the energy-weighted mean photon energy in x_M unit. This treatment of Comptonized synchrotron radiation is almost the same as that adopted in Park & Ostriker (2001), except that the energy enhancement factor is different and the treatment of saturated Comptonization is slightly changed.

In the presence of both bremsstrahlung and synchrotron emission, Λ is replaced by $\Lambda_{Cbr} + \Lambda_{CS}$ in equation (8) and $T_X \Lambda$ by $T_X^{Cbr} \Lambda_{Cbr} + T_X^{CS} \Lambda_{CS}$ in equation (9).

REFERENCES

Abramowicz, M., Chen, X., Kato, S., Lasota, J.-P., & Regev, O. 1995, ApJ, 438, L37
 Ball, G. H., Narayan, R., & Quataert, E. 2001, ApJ, 552, 221 (BNQ)
 Begelman, M. C., & Meyer, D. L. 1982, ApJ, 253, 873
 Blandford, R. D., & Begelman, M. C. 1999, MNRAS, 303, L1
 Ciotti, L., & Ostriker, J. P. 1997, ApJ, 487, L105
 Ciotti, L., & Ostriker, J. P. 2001, ApJ, 551, 131
 Cowie, L. L., Ostriker, J. P., and Stark, A. A. 1978, ApJ, 226, 1041
 Dermer, C. D., Liang, E. P., & Canfield, E. 1991, ApJ, 369, 410

Ichimaru, S. 1997, *ApJ*, 214, 840

Igumenshchev, I. V., & Abramowicz, M. A. 1999, *MNRAS*, 303, 309

Igumenshchev, I. V., & Abramowicz, M. A. 2000, *ApJS*, 130, 463

Igumenshchev, I. V., Abramowicz, M. A., & Narayan, R. 2000, *ApJ*, 537, L27

Igumenshchev, I. V., Chen, X., & Abramowicz, M. A. 1996, *MNRAS*, 278, 236

Levich, E. V. & Syunyaev, R. A. 1971, *Soviet Astronomy*, 15, 363

Mahadevan, R., Narayan, R., & Yi, I. 1996, *ApJ*, 465, 327

Narayan, R., Barret, D., & McClintock, J. E. 1997, *ApJ*, 482, 448

Narayan, R., Igumenshchev, I. V., & Abramowicz, M. A., 2000, *ApJ*, 539, 798 (NIA)

Narayan, R., Mahadevan, R., & Quataert 1999, in *The Theory of Black Hole Accretion Discs*, eds. M. A. Abramowicz, G. Bjornsson, and J. E. Pringle (Cambridge: Cambridge U. Press), 148 (astro-ph/9803141)

Narayan, R., & Yi, I. 1994, *ApJ*, 428, L13

Narayan, R., & Yi, I. 1995a, *ApJ*, 444, 231

Narayan, R., & Yi, I. 1995b, *ApJ*, 452, 710

Nobili, L., Turolla, R., & Zampieri, L. 1991, *ApJ*, 383, 250

Ostriker, J. P., McCray, R., Weaver, R., & Yahil, A. 1976, *ApJ*, 208, L61

Pacholczyk, A. G. 1970, *Radio Astrophysics* (San Francisco: Freeman)

Park, M.-G. 1990a, *ApJ*, 354, 64

Park, M.-G. 1990b, *ApJ*, 354, 83

Park, M.-G. & Ostriker, J. P. 1999, *ApJ*, 527, 247

Park, M.-G. & Ostriker, J. P. 2001, *ApJ*, 549, 100

Quataert, E., & Gruzinov, A. 2000, *ApJ*, 539, 809 (QG)

Rees, M. J., Begelman, M. C., Blanford, R. D., & Phinney, E. S. 1982, *Nature*, 295, 17

Shakura, N. I., & Sunyaev, R. A. 1973, *A&A*, 24, 337

Stepney, S., & Guilbert, P. W. 1983, *MNRAS*, 204, 1269

Stone, J. M., Pringle, J. E., & Begelman, M. C. 1999, *MNRAS*, 310, 1002

Svensson, R. 1982, *ApJ*, 258, 335

Svensson, R. 1984, *MNRAS*, 209, 175

Wandel, A., Yahil, A., & Milgrom, M. 1984, *ApJ*, 282, 53

Xu, G., & Chen, X. 1997, ApJ, 489, L29

Zampieri, L., Miller, J. C., & Turolla, R. 1996, MNRAS, 281, 1183

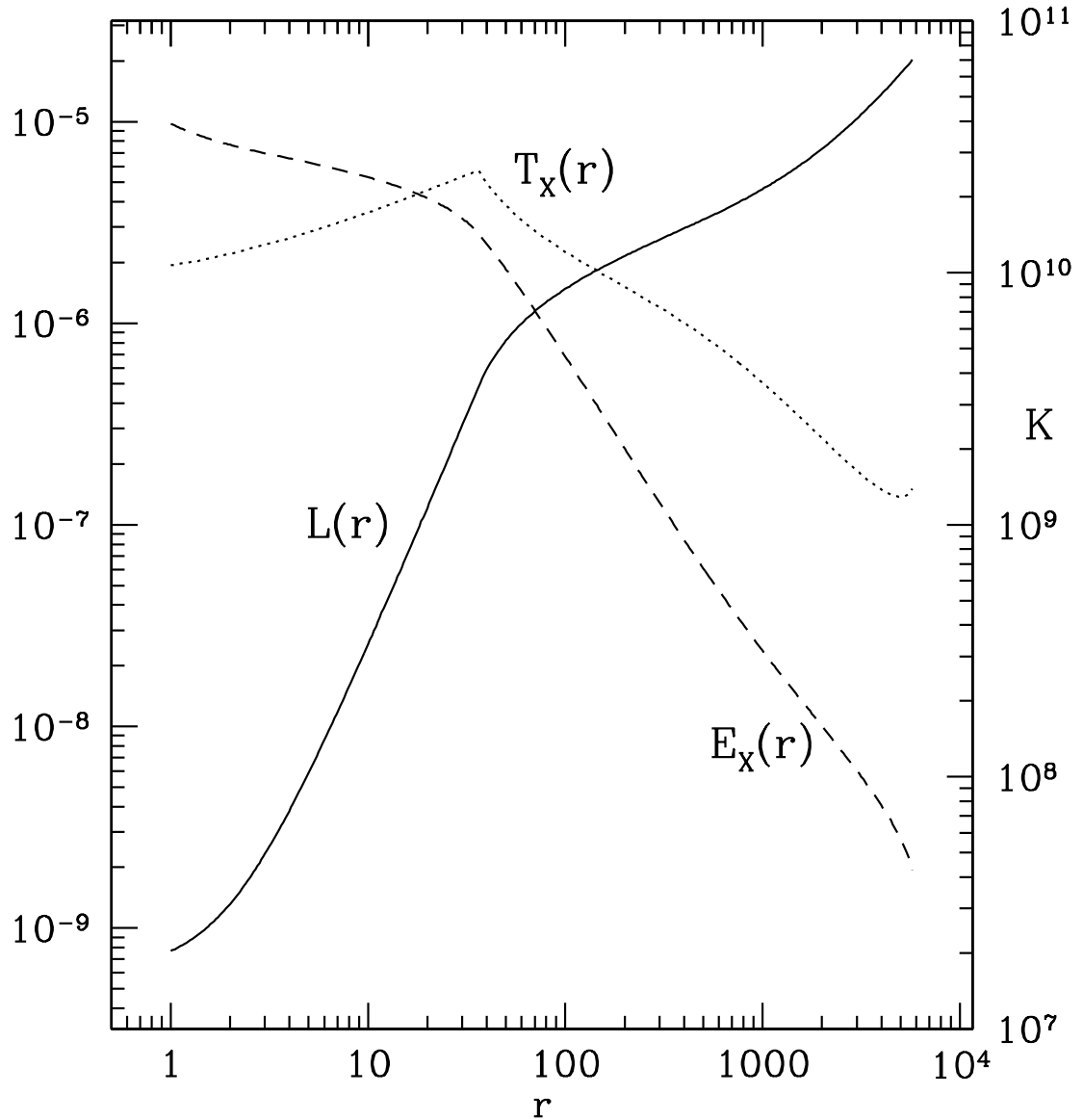


Fig. 1.— The log profiles of luminosity $L(r)$ (in units of L_E , left ordinate), of the radiation energy density $E_X(r)$ (in arbitrary units, left ordinate), and of the radiation temperature $T_X(r)$ (in K, right ordinate).

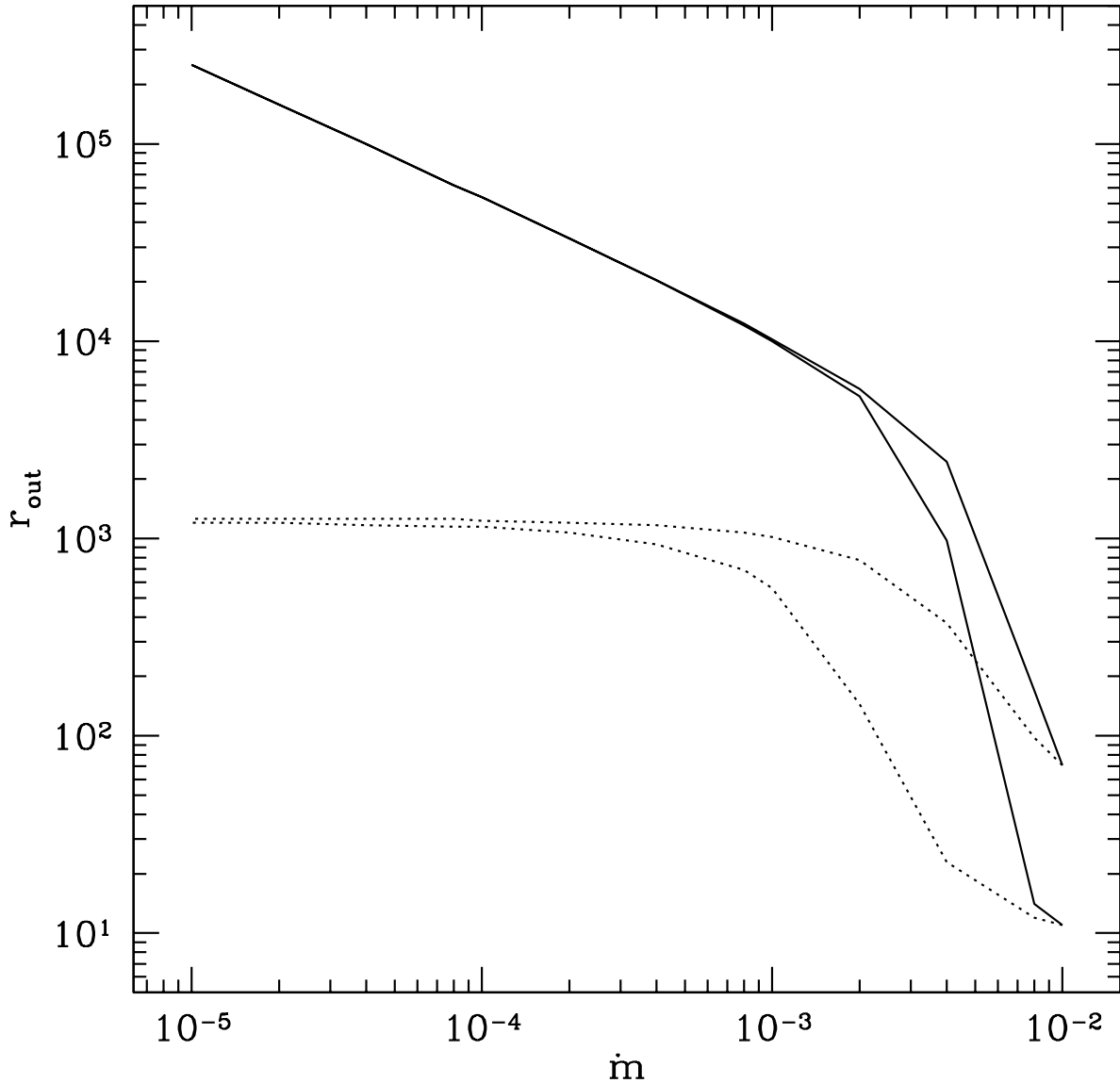


Fig. 2.— The outer boundary radius r_{out} as a function of \dot{m} . *Upper solid line* is for $T_1 = 3 \times 10^{10}$ K and *lower one* for $T_1 = 10^{11}$ K, both for constant radiation efficiency $\epsilon_c \eta_c = 0.01$. *Dotted lines* represent the same r_{out} for varying radiation efficiency $\epsilon_c \eta_c = 10^{-2}(\dot{m}/10^{-2})$: *upper one* for $T_1 = 3 \times 10^{10}$ K and *lower one* for $T_1 = 10^{11}$ K.

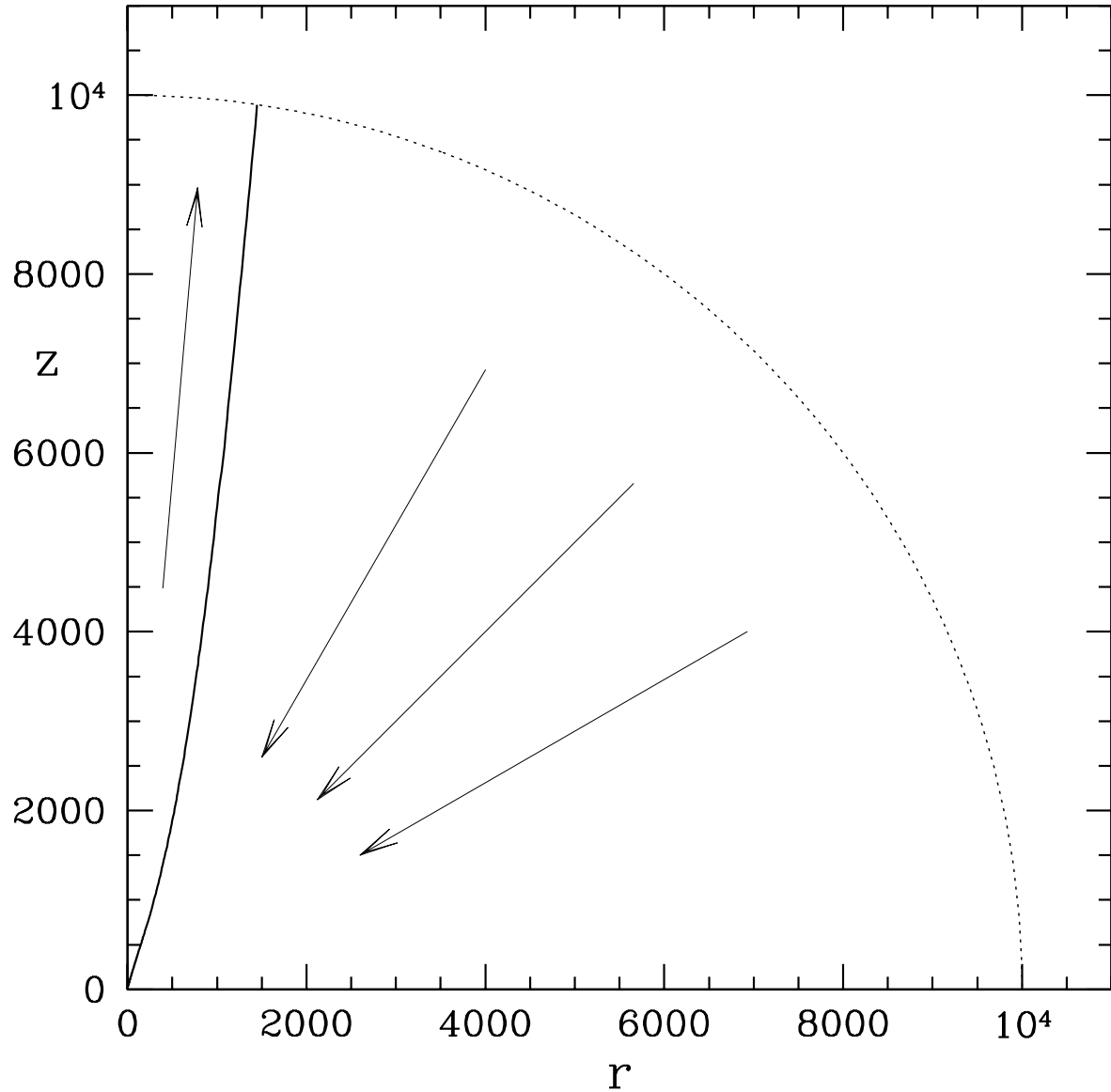


Fig. 3.— The region inside the *solid curve* toward the pole is overheated above the virial temperature due to Compton heating. Outer *dotted circle* shows the outer boundary of CDAF for given total luminosity. This figure is for $\dot{m} = 10^{-3}$ and $T_1 = 10^{11}$ K. The opening angle of the outflow at the outer boundary is only 8° .

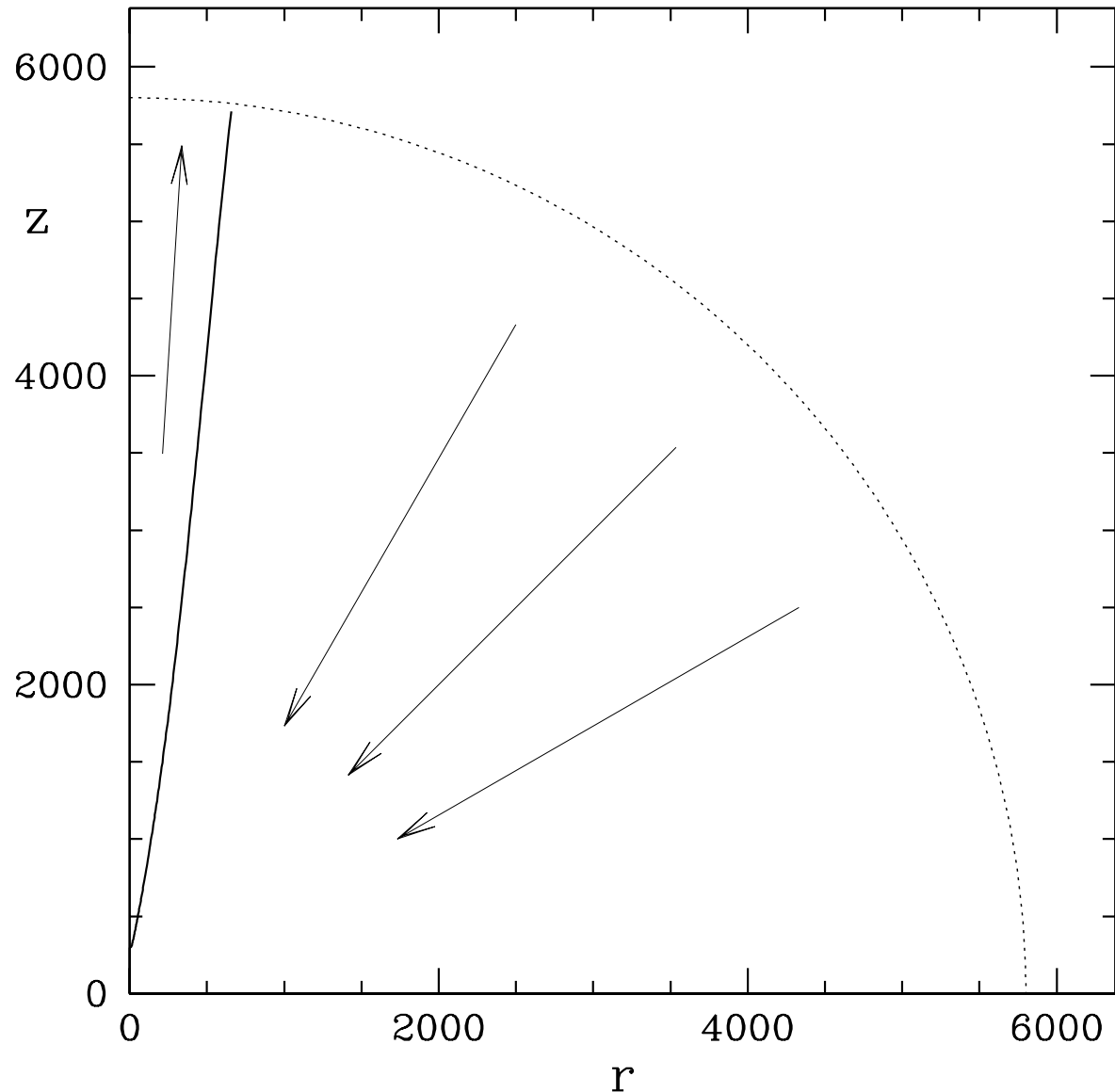


Fig. 4.— Same as Figure 3, but for $\dot{m} = 2 \times 10^{-3}$ and $T_1 = 3 \times 10^{10}$ K. The opening angle at the outer boundary is 8° .

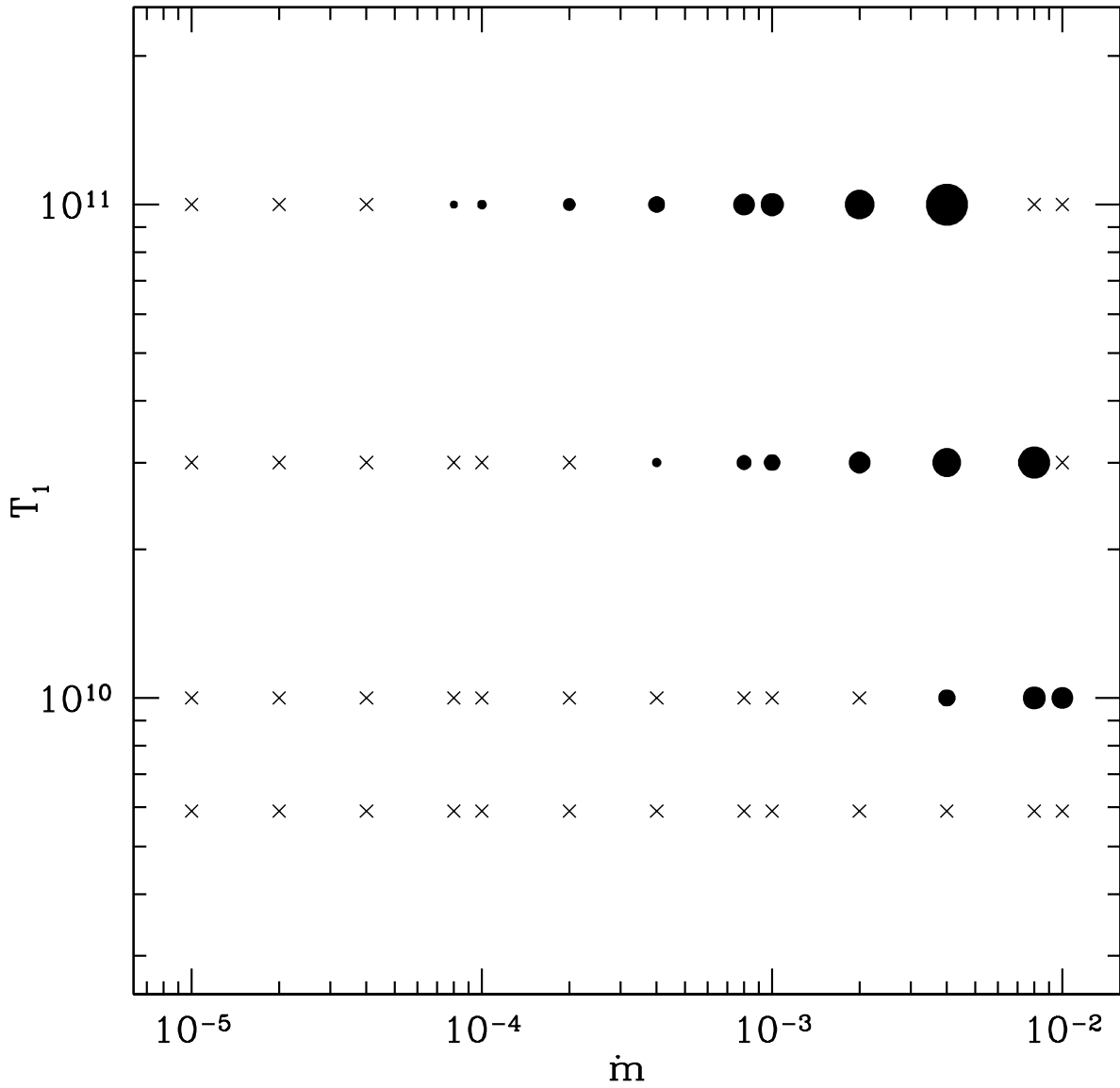


Fig. 5.— The parameter space of (\dot{m}, T_1) under constant radiation efficiency for which outflow exists is denoted as circles. The size of circle represents the opening angle of the outflow at the outer boundary. No outflow is found at (\dot{m}, T_1) denoted by crosses.

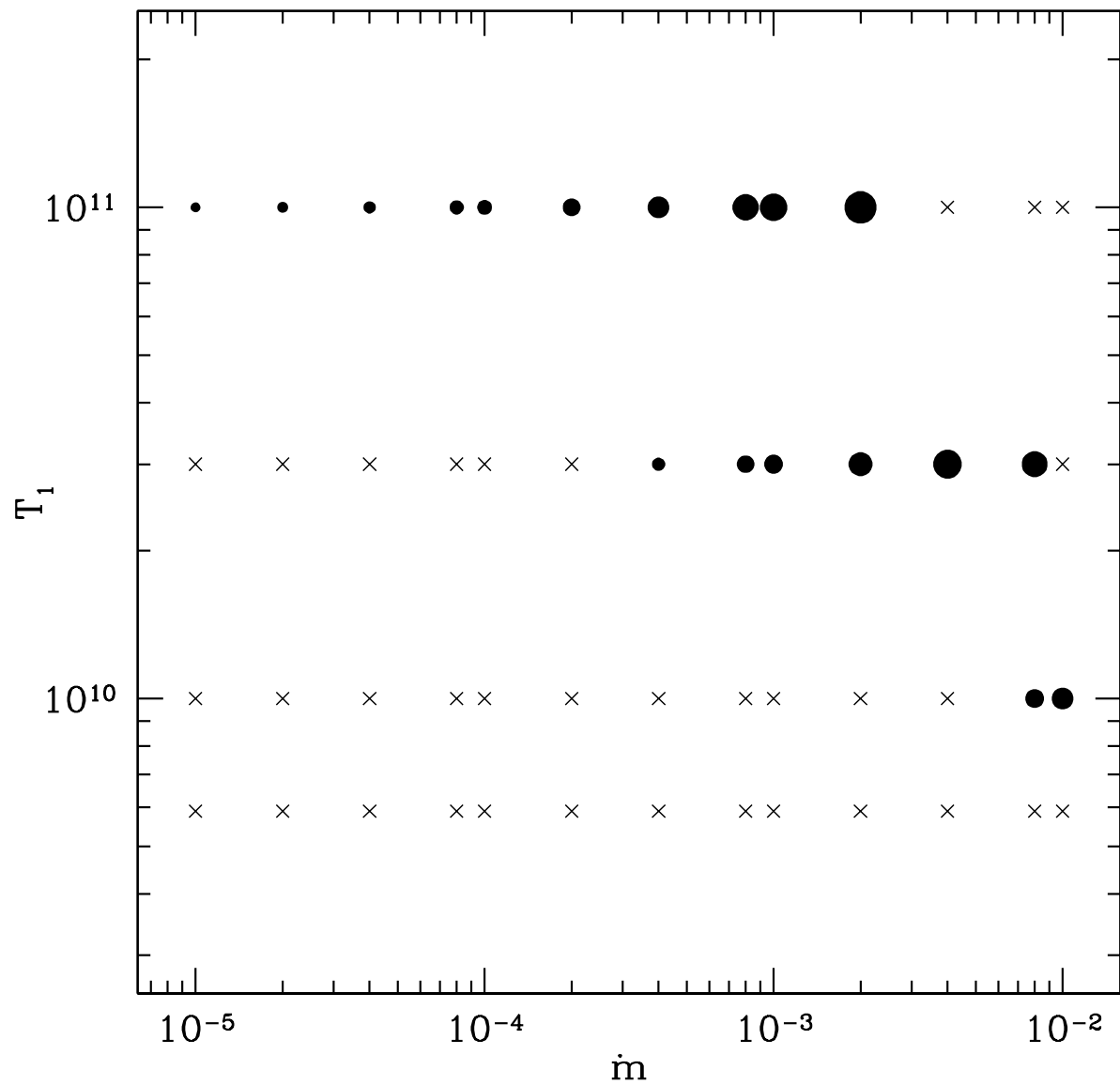


Fig. 6.— Same as Figure 5, but now the radiation efficiency is proportional to the mass accretion rate.

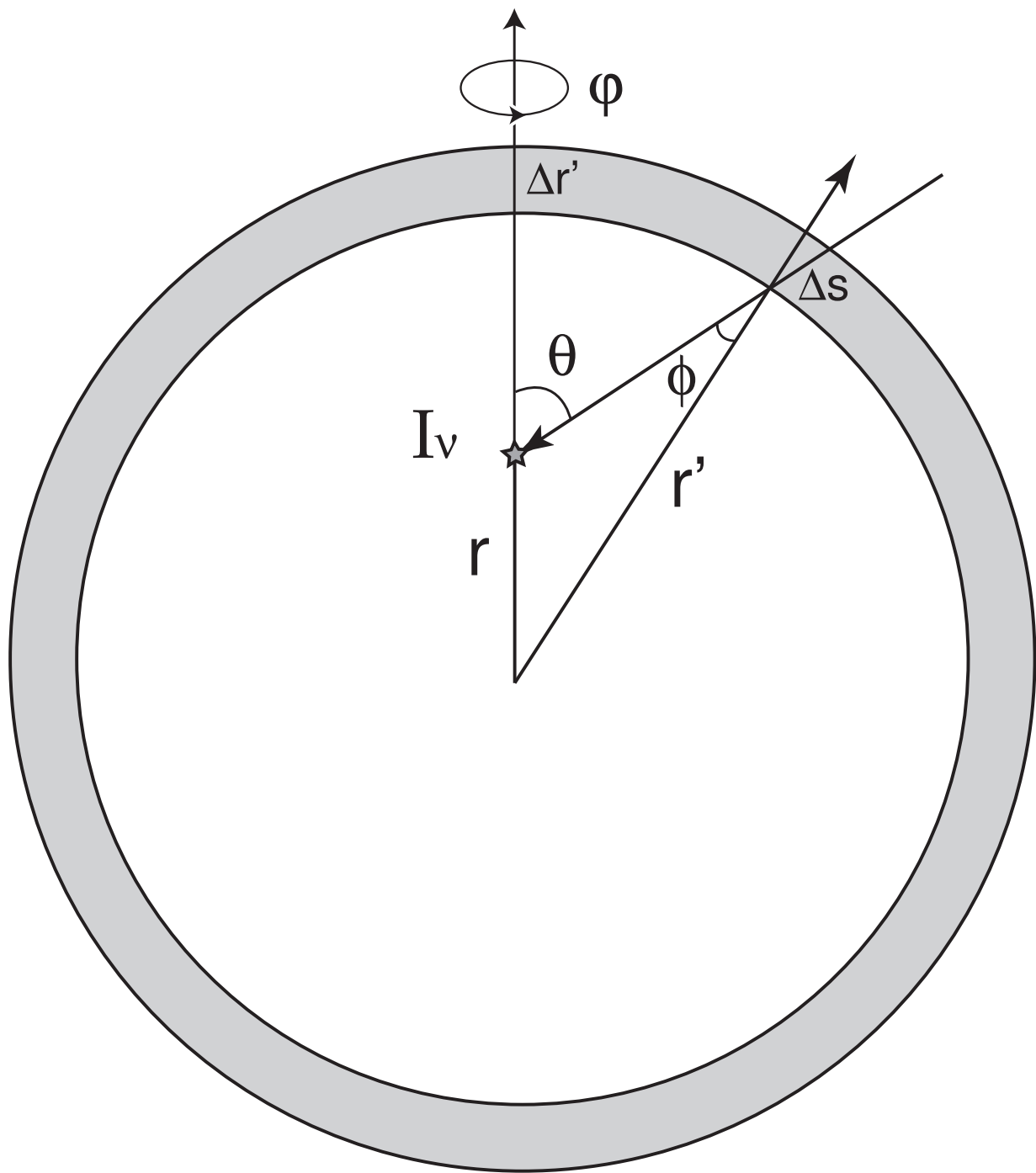


Fig. 7.— The diagram for calculation of specific intensity, I_ν , inside a radiating spherical shell.